

Understanding molecular representations in machine learning: The role of uniqueness and target similarity

Bing Huang and O. Anatole von Lilienfeld*

*Institute of Physical Chemistry and National Center for Computational Design and Discovery of Novel Materials (MARVEL),
Department of Chemistry, University of Basel, Klingelbergstrasse 80, 4056 Basel, Switzerland*

(Dated: September 1, 2016)

The predictive accuracy of Machine Learning (ML) models of molecular properties depends on the choice of the molecular representation. Based on the postulates of quantum mechanics, we introduce a hierarchy of representations which meet uniqueness and target similarity criteria. To systematically control target similarity, we rely on interatomic many body expansions, as implemented in universal force-fields, including Bonding, Angular, and higher order terms (BA). Addition of higher order contributions systematically increases similarity to the true potential energy and predictive accuracy of the resulting ML models. We report numerical evidence for the performance of BAML models trained on molecular properties pre-calculated at electron-correlated and density functional theory level of theory for thousands of small organic molecules. Properties studied include enthalpies and free energies of atomization, heatcapacity, zero-point vibrational energies, dipole-moment, polarizability, HOMO/LUMO energies and gap, ionization potential, electron affinity, and electronic excitations. After training, BAML predicts energies or electronic properties of out-of-sample molecules with unprecedented accuracy and speed.

Reasonable predictions of ground-state properties of molecules require computationally demanding calculations of approximated expectation values of the corresponding operators.¹ Alternatively, Kernel-Ridge-Regression (KRR) based machine learning (ML) models² can also *infer* the observable in terms of a linear expansion in chemical compound space^{3,4}. More specifically, an observable can be estimated using $O^{\text{inf}}(\mathbf{M}) = \sum_i^N \alpha_i k(d(\mathbf{M}, \mathbf{M}_i))$, where k is the kernel function (we use Laplacian kernels with training set dependent width), d is a metric (we use the L_1 -norm), and \mathbf{M} is the molecular representation^{5,6}. The sum runs over all reference molecules i used for training to obtain regression weights $\{\alpha_i\}$. Once trained, the advantage of such ML methods consists of (i) their computational efficiency (multiple orders of speed-up with respect to conventional quantum chemistry) and (ii) their accuracy can systematically be converged to complete basis set limit through addition of sufficient training instances. Their drawback is that they (a) are incapable of extrapolation by construction, and (b) require substantial training data before reaching satisfying predictive power for out-of-sample molecules. In practice, addressing (a) is less important since one typically knows beforehand which ranges of interatomic distances and chemical compositions are relevant to the chemical problem at hand: It is straightforward to define the appropriate domain of applicability for the application of supervised ML models in chemistry. In recent years, much work has been devoted to tackle the latter drawback through the discovery and development of improved representations \mathbf{M} ⁷⁻¹³.

Often, new descriptors are introduced based on *ad hoc*/trial-and-error reasoning, such as using features which characterize a system or the property of interest, which meet known invariances, which simply add “more physics”, or which simply encode anything which could possibly be related to the system and property of inter-

est. The use of new representations is justified *a posteriori*: They yield ML models with good performance. Severe survivorship bias, however, might occur: Alternative representations which could have been obtained from the same set of guidelines, and which would result in poor ML model performance, are omitted. While such practice is not wrong it is questionable: Arbitrarily many different representations could have been designed using the exact same guidelines. To the best of our knowledge, there is no general specific and rigorous procedure for systematically optimizing molecular representations for converged and robust ML model performance *without* drawing heavy numerical experimentation and conclusions *a posteriori*. In this paper, we rely on the postulates of quantum mechanics to identify a hierarchy of representations which enable the generation of ML models with systematically increased predictive accuracy. We approximate the hierarchy using universal force-field (UFF) parameters¹⁶. To support our findings, we present numerical evidence for multiple ML models using the same set of quantum chemical ground-state properties and structures, previously calculated for thousands of organic molecules¹⁷

For large N , errors of ML models have been observed to decay as inverse roots of N^2 , implying a linear relationship, $\log(\text{Error}) = a - b \log(N)$. Therefore, the best representation must (i) minimize the off-set a and (ii) preserve the linearity in the second term while maximizing its pre-factor b . According to the first postulate of quantum mechanics any system is represented by its wavefunction Ψ which results from applying the variational principle to the expectation value of the Hamiltonian operator. As such, there is a one-to-one relationship between Hamiltonian and Ψ . While some representations have been introduced in order to mimic Ψ (or its corresponding electron density¹⁸)^{19,20}.

Unfortunately, many observables are extremely sensitive to minute changes in Ψ , as such we prefer to focus

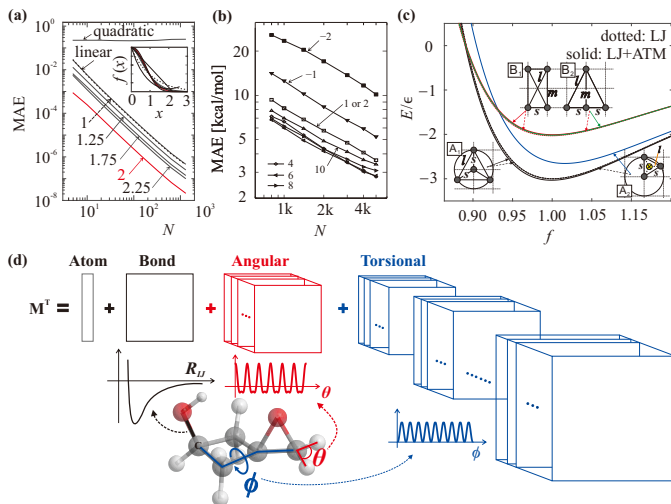


Figure 1. Target similarity determines offset a in ML model learning curves $\log(\text{Error}) = a - b \log(N)$. Panels (a) and (b) illustrate learning curves for ML models obtained for representations of varying target similarity applied to (a) modeling a 1-D Gaussian target function or (b) enthalpy of atomization for QM7b dataset⁶. Lines in (a) correspond to models resulting from linear, quadratic, and various exponential (e^{-x^n} with $n = \{1, 1.25, 1.75, 2 \text{ and } 2.25\}$) representations. The inset shows the target function (red) as well as the representations. Learning curves in (b) correspond to models resulting from Coulomb matrices with varying definition of off-diagonal elements, $Z_I Z_J / R_{IJ}^n$, where n is specified in the figure. (c) Illustration that 3-body interactions are crucial for distinguishing two pairs of homometric Ar_4 clusters: pair A (A_1 and A_2 , where $l = \sqrt{3}s$) and pair B (B_1 and B_2 , where $m = 2s, l = \sqrt{5}s$). Horizontal axis label f scales s , where $f = 1$ corresponds to the choice $s = 3.82 \text{ \AA}$. LJ and ATM correspond to Lennard-Jones and Axilrod-Teller-Muto^{14,15} potentials, respectively. (d) Illustration of the universal force-field¹⁶ based construction of the BA representation.

directly on the system’s Hamiltonian (and the potential energy surface it defines) defined in chemical compound space⁴. We have realized that representations based on increasingly more accurate approximations to the potential energy surface afford increasingly more accurate KRR ML models. In other words, as between representation and potential energy (target similarity) increases the off-set a in the linear log – log learning curve decreases. Furthermore, b appears to be a global constant, independent of the representation’s target similarity, as long as the crucial¹⁰ uniqueness criterion is met.

First, we exemplify the importance of target similarity for a mock supervised learning task: Modeling a 1D Gaussian function (Inset Fig. 1(a)). As representations \mathbf{M} we use linear, quadratic, and exponentially decaying functions with varying exponent of x . Learning curves of resulting ML models (Fig. 1(a)) indicate systematic improvement as the target similarity, i.e. similarity of representation to Gaussian function, increases. Note that all learning curves, with the notable exception of the quadratic one, exhibit the same slope b on the log-log

plot of the learning curve: They only differ in learning curve off-set a which co-incides with their target similarity. When using a Gaussian function as a representation, the smallest off-set is observed—as one would expect. It is easy to see why the error of the ML model using the quadratic function as a representation does not decrease when adding more training data: Its minimum is at $x = 2$, and in the region $x > 2$ the function turns upward again, preventing a one-to-one map between x and representation. In other words, the quadratic function is not monotonic and therefore lacks uniqueness, introducing noise in the data which can not converge to zero and which results in a constant error for large N . By contrast, all other representations are monotonic and conserve the one-to-one map to x . As such, they are unique representations and they all reduce the logarithm of the error in a linear fashion at the same rate as the amount of training data grows. While the rate appears to be solely determined by the uniqueness of the representation, confirming that uniqueness is a necessary condition for functional descriptors⁴, the off-set a of the resulting learning curve appears to be solely determined by target similarity.

To see if our line of reasoning also holds for real molecules, we have investigated the performance of ML models for predicting atomization energies of organic molecules using a set of unique representations with differing target similarity. More specifically, we calculated learning curves for ML models resulting from atom adjacency matrices derived from the Coulomb matrix⁵, with off-diagonal elements $M_{IJ} = Z_I Z_J / R_{IJ}^n$. Where R_{IJ} is the interatomic distance between atoms I and J , and the conventional variant (giving rise to the name) is recovered for $n = 1$. For any non-zero choice of n these matrices encode the complete polyhedron defined in the high-dimensional space spanned by all atoms in the molecules: They uniquely encode the molecule’s geometry and composition, thereby ensuring a constant b . For negative n values, however, this representation becomes an unphysical model of the atomization energy: The magnitude of its off-diagonal elements *increases* with interatomic distance. Corresponding learning curves shown in Fig. 1(b) reflect this fact: As off-diagonal elements become increasingly unphysical by dialing in square-root, linear, and quadratic functions in interatomic distance, respectively, the off-set a increases. Conversely, matrix representations with off-diagonal elements which follow the Coulomb and higher inverse power laws are more physical and exhibit lower off-sets. Interestingly, we note the additional improvement as we change from Coulombic $1/R$ to van der Waals $1/R^6$ like power laws. These results suggest that—after scaling—pairwise London dispersion kind of interactions are more similar to molecular atomization energies than simple Coulomb interactions. In the following, we dubb the resulting representation the London Matrix (LM).

The bag-of-bond (BoB) representation, a stripped down pair-wise variant of the Coulomb matrix, has re-

sulted in remarkably predictive ML models²¹. Starting with the insights gained from the above, we use the bagging idea as a starting point for the development of our systematically improved representation. Unfortunately, when relying on bags of pair-wise interactions as a representation the uniqueness requirement is violated by arbitrarily many sets of geometries, no matter how strong the (effective) target similarity of the employed functional form. In Fig. 1(d), we demonstrate this issue for two pairs of homometric molecules, each with four rare gas atoms, and once in a competition of a pyramidal/planar geometry (A), and once for a rectangular/triangular pair (B). Both pairs exhibit the exact same list of interatomic distances: $3 s/3 l$ for A, and $2 s/2 m/2 l$ for B. Consequently, when using a pair-wise energy expression (no matter how effective), the predicted curve as a function of a global scaling factor f will be indistinguishable for both pairs (example shown in Fig. 1(d) using Lennard-Jones potentials with parameters for Argon). Only after the addition of the corresponding three-body van der Waals Axilrod-Teller-Muto^{14,15} contribution, the homometric pairs can be distinguished²².

Using the insight gained, we have investigated a hierarchy of representations which consists of bags of (1) dressed atoms (\mathbf{M}^D), (2) atoms and bonds (\mathbf{M}^B), (2) atoms, bonds and angles (\mathbf{M}^A), and (3) atoms, bonds, angles, and torsions (\mathbf{M}^T). To indicate the many-body expansion character we dubb these feature vectors “BA-representation” (standing for bags of Bonds, Angles, Torsions, etc. pp.). Here, we have chosen functional forms and parameters for BA-representations that correspond to UFF¹⁶. The corresponding terms are illustrated in Fig. 1(d), and correspond to averaged atomic contributions to energies of molecules in training set for atoms, Morse and Lennard-Jones potentials for covalent and non-covalent intramolecular bonding, respectively, as well as sinusoidal functions for angles and torsions. More technical details regarding the training can be found in the supplementary materials. While we find that use of the UFF results in consistent and remarkable performance, we note that other force fields could have been used just as well. In particular, we also tested Lennard-Jones and Axilrod-Teller-Muto potentials in BA based ML models (BAML), and found systematic improvement and similar performance also for these functional forms and parameters.

We tested UFF based BAML using three previously established data sets: DFT energies and properties of $\sim 7k$ organic molecules stored in the QM7b data set⁶, G4MP2 energies and DFT properties for 6k constitutional isomers of $C_7H_{10}O_2$, and DFT energies and properties for 134k organic molecules QM9 (both published in Ref.¹⁷). Links to all data sets are available at <http://quantum-machine.org>. Initial structures for all datasets were drawn from the GDB universe^{29,30}.

Log-log plots of BAML learning curves are shown in Fig. 2(a) and (b) for the $C_7H_{10}O_2$ isomers as well as for QM9. Mean absolute errors (MAEs) for out of sample

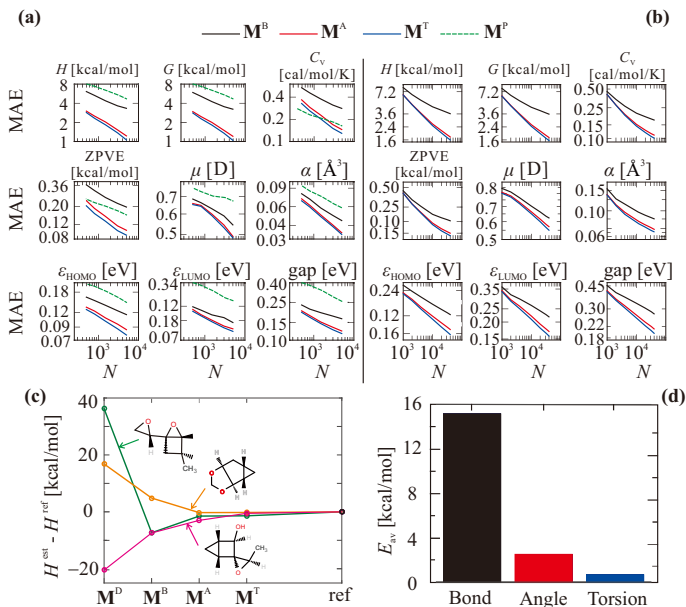


Figure 2. (a): BAML and polarizability representation based ML learning curves for 9 molecular properties of 6k constitutional isomers of formula $C_7H_{10}O_2$ ¹⁷. (b) BAML learning curves for 134k QM9 molecules for the same 9 molecular properties¹⁷. Property models cover H , G , C_V , ZPVE, μ , α , ϵ_{HOMO} and ϵ_{LUMO} , i.e. enthalpy, free energy, heat capacity, zero point vibrational energy, dipole moment, polarizability, HOMO and LUMO energy, respectively. Panel (c) shows convergence of estimated enthalpy values to reference values (all shifted to zero) for three most extreme outlier isomers in $C_7H_{10}O_2$ set. Panel (d) is the averaged “contribution” of each order type in a many-body potential, i.e., the bond, angle and torsion part.

predictions of nine properties are shown as a function of training set size for the BAML model. Properties studied include enthalpies and free energies of atomization at room temperature, heat-capacity at room temperature C_V , zero-point-vibrational-energy (ZPVE), norms of dipole moments μ and polarizability α , as well as HOMO/LUMO eigenvalues and gap. For any given property, we find near identical learning rates among BAML models based on bonds (\mathbf{M}^B), bonds+angles (\mathbf{M}^A), or atoms+bonds, angles+torsions (\mathbf{M}^T), respectively. The learning off-set a , however, decreases systematically as target similarity to energy is being increased through the addition of higher order contributions—for all properties, and for both data sets. We note that BAML can reach chemical accuracy (MAE ~ 1 kcal/mol with respect to reference) for atomization energies of the isomers of $C_7H_{10}O_2$ after training on only 5k example molecules, and MAE ~ 2.4 kcal/mol for 134k organic molecules in QM9 after training on 10k example molecules. To the best of our knowledge, such predictive power has not yet been reached by any other ML model. This observation confirms the expectations raised based on the aforementioned arguments.

In Fig. 2(c) individual contributions to the atomization

Table I. Mean absolute errors and root mean square errors in brackets) for the ML predictions of 14 molecular properties of molecules in QM7b data set⁶. Results from this work (BAML, BoB, BoL, CM, LM) are shown together with previously published estimation (SOAP¹⁹, rand CM⁶) for the same dataset. Errors are measured on test set of 2200 randomly selected configurations, while the remaining compounds out of QM7b were used for training. Labels specify property and level of theory: Atomization energy (E), averaged molecular polarizability (α), HOMO and LUMO eigenvalues, ionization potential (IP), electron affinity (EA), first excitation energy (E_{1st}^*), excitation frequency of maximal absorption (E_{max}^*) and the corresponding maximal absorption intensity (I_{max}). Expected averaged deviation from experiment is specified in the last column.

| property | SD | BAML | BoB | BoL | CM | LM | SOAP ¹⁹ | rand CM ⁶ | accuracy |
|------------------------------------|--------|--------------------|----------------------|-------------|-------------|-------------|--------------------|----------------------|--|
| E (PBE0) [kcal/mol] | 223.69 | 1.15 (2.54) | 1.84 (4.15) | 1.77 (4.07) | 3.69 (5.77) | 2.84 (4.94) | 0.92 (1.61) | 3.69 (8.30) | 3.46 ^a , 5.30 ^b , 2.08-5.07 ^c |
| α (PBE0) [\AA^3] | 1.34 | 0.07 (0.12) | 0.09 (0.13) | 0.10 (0.15) | 0.13 (0.19) | 0.15 (0.20) | 0.05 (0.07) | 0.11 (0.18) | 0.05-0.27 ^d , 0.04-0.14 ^e |
| HOMO (GW) [eV] | 0.70 | 0.10 (0.16) | 0.15 (0.20) | 0.15 (0.20) | 0.22 (0.29) | 0.20 (0.26) | 0.12 (0.17) | 0.16 (0.22) | - |
| LUMO (GW) [eV] | 0.48 | 0.11 (0.16) | 0.16 (0.22) | 0.16 (0.22) | 0.21 (0.27) | 0.19 (0.25) | 0.12 (0.17) | 0.13 (0.21) | - |
| IP (ZINDO) [eV] | 0.96 | 0.15 (0.24) | 0.20 (0.28) | 0.20 (0.28) | 0.33 (0.44) | 0.31 (0.41) | 0.19 (0.28) | 0.17 (0.26) | 0.20, 0.15 ^d |
| EA (ZINDO) [eV] | 1.41 | 0.07 (0.12) | 0.17 (0.23) | 0.18 (0.24) | 0.31 (0.40) | 0.25 (0.33) | 0.13 (0.18) | 0.11 (0.18) | 0.16 ^f , 0.11 ^d |
| E_{1st}^* (ZINDO) [eV] | 1.87 | 0.13 (0.51) | 0.21 (0.30) | 0.22 (0.31) | 0.42 (0.57) | 0.35 (0.46) | 0.18 (0.41) | 0.13 (0.31) | 0.18 ^f , 0.21 ^g |
| E_{max}^* (ZINDO) [eV] | 2.82 | 1.35 (1.98) | 1.40 (1.91) | 1.47 (2.02) | 1.58 (2.05) | 1.68 (2.20) | 1.56 (2.16) | 1.06 (1.76) | - |
| I_{max} (ZINDO) | 0.22 | 0.07 (0.11) | 0.08 (0.12) | 0.08 (0.12) | 0.09 (0.13) | 0.09 (0.13) | 0.08 (0.12) | 0.07 (0.12) | - |

^a MAE of formation enthalpy for the G3/99 set by PBE0^{23,24}; ^b MAE of atomization energy (AE) for 6 small molecules^{25,26} by PBE0; ^c MAE of AE from various studies²⁷ by B3LYP; ^d MAE from various studies²⁷ by B3LYP; ^e MAE from various studies by MP2²⁷; ^f MAE for the G3/99 set by PBE0^{23,24}; ^g MAE for a set of 17 retinal analogues by TD-DFT(PBE0)²⁸.

energy are on display, resulting from bonds, angles, and torsion representations. For illustration, we have selected outliers, i.e. three constitutional isomers of $C_7H_{10}O_2$ for which the out-of-sample prediction error is maximal. In all three cases, these molecules experience high internal strain through few membered or joint hetero cycles. As such, it is reassuring to observe substantial lowering of the error occurs as soon as the representation accounts explicitly for angular and torsional degrees of freedom. Fig. 2(d) indicates averaged changes obtained for the entire constitutional isomer testing set due to addition of higher order terms to the representation. More specifically, addition of bonds to dressed atoms contributes ~ 15 kcal/mol; augmenting the representation by angular degrees of freedom reduces this number to ~ 2 kcal/mol; while further addition of torsional degrees of freedom improves results by merely ~ 0.5 kcal/mol. Note that the last change might be small on average, however, for some molecules it can be consequential if high accuracy shall be achieved, e.g. in the case of outliers shown in Fig. 2(c). Overall, it is encouraging to see that these contributions decrease systematically. These results suggest that ML models of energies converge rapidly in the many-body expansion of representations. This finding indicates that it should be possible to construct local ML models which scale linearly with system size.

Having established uniqueness and target similarity criteria, we now discuss the choice to represent molecules in terms of bags of interatomic many-body energy expansion. This choice is not evident, many representations used in the literature rely on the use of additional properties, such as HOMO/LUMO eigenvalues, or atomic radii and spectra. For two reasons we believe an energy based representation to be advantageous: First, energy is the very observable associated to the Hamiltonian which defines the system: The potential energy surface of a given molecular electronic spin-state is equally and uniquely

representative for the system: Two different systems will always differ in their potential energy surface. Secondly, energy is well understood and there is a large choice of decent energy models, such as UFF, which can be used for constructing good representations. It is not easy to construct good models of other properties which at the same time also meet the uniqueness criterion. For example, for comparison we constructed a molecular representation which reaches high target similarity with another property, polarizability. Instead of using bags of interatomic energy contributions we have used a bag of atomic polarizabilities. Atomic polarizabilities can easily be obtained from Cartesian coordinates of a molecule, i.e. without electronic structure calculations, through the use of Voronoi polyhedra.³¹ Unfortunately, this representation violates the uniqueness criterion. While (M^P) is a decent model of molecular polarizability it is not unique: Any other molecule which happens to have the same set of atomic volumes, irrespective of differences in geometry, will result in the same representation. Learning curves obtained for M^P based ML models are shown together with BAML in Fig. 2(a) for all constitutional isomers. All hierarchies of BAML models have lower learning curves for all properties except ZPVE and C_V for which the bond based BAML models perform slightly worse. In the case of the latter, and for very small unconverged training set sizes, the polarizability ML model is even better than any BAML model, however, as training set size grows the lack of uniqueness kicks in with a more shallow learning rate leading to worse performance. This observation also underscores the necessity to take the convergence behavior of ML models into consideration: Learning behavior can differ in *a* and *b*. We note the tendency of the polarizability based ML model towards a smaller slope (C_V , ZPVE, μ , α), indicating the expected lack of uniqueness. Surprisingly, even for the target property polarizability M^P based ML models show worse performance than any

BAML model. These numerical results support the idea that Hamiltonian/ Ψ /Potential Energy Surface are “special” in that all other molecular properties can be derived from them, in direct analogy to the wavefunction Ψ , necessary to calculate the corresponding expectation values.

Finally, to place the BAML performance into perspective, we have also compared the out-of-sample errors for its most accurate variant to literature results obtained using alternative ML models and representations applied to the same molecular data set, QM7b⁶. Tab. I displays MAEs and RMSE of the \mathbf{M}^T based BAML model trained on 5k molecules, as well as London Matrix (LM), Coulomb Matrix (CM), BoB (which is a bag of Coulomb matrix elements), and bag of London (BoL) matrix elements. In particular, we compare to results from this work with SOAP¹⁹, and randomized neural network based CM model⁶. SOAP represents a recently introduced sophisticated convolution of kernel, metric and representation. We note that by no means this represents a comprehensive assessment, it would have been preferable to compare learning curves, such as in Fig. 2 (a) and (b). However, the implementation of SOAP or neural network models can be complex and is beyond the scope of this study. BAML yields a MAE for atomization energy of only ~ 1.15 kcal/mol, only slightly worse than SOAP’s ~ 0.92 kcal/mol. We consider such small differences to be negligible for all intents and purposes: Differences between QM codes due to use of different compilers, libraries, or optimizers can reach similar scale. We also note, however, in Tab. I that BAML has a considerably larger RMSE (2.5 kcal/mol) for the atomization energy than SOAP (1.6 kcal/mol). Similar observations hold for the polarizability. For HOMO/LUMO eigenvalues, ionization potential, electron affinity, and the intensity of the most intense peak, BAML yields lowest MAE and lowest RMSE. BAML also has the lowest MAE for predicting the first excitation energy (together with the randomized neural network based Coulomb matrix model). The lowest RMSE for this property, however, is obtained using a BOB based ML model. The excitation energy of the most intense peak in the model is predicted with the lowest MAE and RMSE when using the randomized neural network based Coulomb matrix model. BAML is second for MAE, and third for RMSE (after BoB). To further illustrate the effect of target similarity, we also report BoL vs. BoB and LM vs. CM based results. For most properties, not only the energy, the corresponding London variant outperforms the Coulomb element based ML models. This finding supports the observations made

above that (a) London is more more similar to atomization energy than Coulomb, and (b) the more similar the representation to energy, the more transferable and applicable it is for other properties.

In conclusion, we have presented arguments and numerical evidence in support of the notion that a and $b \log N$ in learning curves are influenced, if not determined, by the employed representation’s target similarity and uniqueness, respectively. For molecules, defined by their Hamiltonian which produces their wavefunction which produces the observables, BAML models—based on universal force-field parameters and functions for bags of bonds, angles, and torsions—exhibit uniqueness as well as considerable similarity to energy. As a result, BAML performs universally well for the modeling of *all* simple scalar global quantum mechanical observables. Addition of higher-order contributions in the form of bonds, angles, and torsional degrees of freedom enables the systematic lowering of learning curve off-set a , resulting in BAML models with unprecedented accuracy, transferability, and speed. Finally, we would like to note that it is possible to define a Pareto front based on the established learning curves, for which the logarithm of the error decays as $a - b \log N$, and the presented uniqueness and target similarity criteria. The front is spanned between error and chemical space. It negotiates the optimal trade-off between number of training instances (or CPU budget in the case of quantum chemistry calculations) and permissible error. As such, it is akin to basis set or electron correlation convergence plots, where for a given computational budget the maximal accuracy can be dialed in, or where, conversely, for a given desired accuracy, the necessary computational budget can be estimated. This latter aspect might be relevant to the automatized generation of QM derived property models with predefined uncertainty and transferability.

ACKNOWLEDGMENTS

O.A.v.L. acknowledges funding from the Swiss National Science foundation (No. PP00P2.138932, 310030.160067). This research was partly supported by the NCCR MARVEL, funded by the Swiss National Science Foundation. Calculations were performed at sci-CORE (<http://scicore.unibas.ch/>) scientific computing core facility at University of Basel.

* anatole.vonlilienfeld@unibas.ch

¹ A. Szabo and N. S. Ostlund, *Modern quantum chemistry: introduction to advanced electronic structure theory* (Courier Corporation, 1989).

² K.-R. Müller, M. Finke, N. Murata, K. Schulten, and S. Amari, *Neural Computation* **8**, 1085 (1996).

³ P. Kirkpatrick and C. Ellis, *Nature* **432**, 823 (2004).

⁴ O. A. von Lilienfeld, *International Journal of Quantum Chemistry* **113**, 1676 (2013).

⁵ M. Rupp, A. Tkatchenko, K.-R. Müller, and O. A. von Lilienfeld, *Physical Review Letters* **108**, 058301 (2012).

⁶ G. Montavon, M. Rupp, V. Gobre, A. Vazquez-Mayagoitia,

- K. Hansen, A. Tkatchenko, K.-R. Müller, and O. A. von Lilienfeld, *New Journal of Physics* **15**, 095003 (2013).
- ⁷ J. Behler, *The Journal of Chemical Physics* **134**, 074106 (2011).
- ⁸ A. P. Bartók, R. Kondor, and G. Csányi, *Phys. Rev. B* **87**, 184115 (2013).
- ⁹ K. T. Schütt, H. Glawe, F. Brockherde, A. Sanna, K. R. Müller, and E. K. U. Gross, *Phys. Rev. B* **89**, 205118 (2014).
- ¹⁰ O. A. von Lilienfeld, R. Ramakrishnan, M. Rupp, and A. Knoll, *International Journal of Quantum Chemistry* **115**, 1084 (2015).
- ¹¹ L. M. Ghiringhelli, J. Vybiral, S. V. Levchenko, C. Draxl, and M. Scheffler, *Phys. Rev. Lett.* **114**, 105503 (2015).
- ¹² F. Faber, A. Lindmaa, O. A. von Lilienfeld, and R. Armiento, *International Journal of Quantum Chemistry* **115**, 1094 (2015).
- ¹³ V. Botu and R. Ramprasad, *International Journal of Quantum Chemistry* **115**, 1074 (2015).
- ¹⁴ B. M. Axilrod and E. Teller, *The Journal of Chemical Physics* **11**, 299 (1943).
- ¹⁵ Y. Muto, *J. Phys.-Math. Soc. Japan.* **17**, 629 (1943).
- ¹⁶ A. K. Rappe, C. J. Casewit, K. S. Colwell, W. A. G. III, and W. M. Skiff, *Journal of the American Chemical Society* **114**, 10024 (1992).
- ¹⁷ R. Ramakrishnan, P. O. Dral, M. Rupp, and O. A. von Lilienfeld, *Scientific Data* **1**, EP (2014).
- ¹⁸ P. Hohenberg and W. Kohn, *Phys. Rev.* **136**, B864 (1964).
- ¹⁹ S. De, A. P. Bartok, G. Csanyi, and M. Ceriotti, *Phys. Chem. Chem. Phys.* **18**, 13754 (2016).
- ²⁰ M. Hirn, S. Mallat, and N. Poilvert, (2016), <http://arxiv.org/abs/1605.04654>.
- ²¹ K. Hansen, F. Biegler, R. Ramakrishnan, W. Pronobis, O. A. von Lilienfeld, K.-R. Müller, and A. Tkatchenko, *The Journal of Physical Chemistry Letters* **6**, 2326 (2015).
- ²² This simple example also underscores the qualitative importance of many-body contributions in interatomic energy decompositions which play a role even in effects as weak as London dispersion forces—in addition to the already established quantitative role they play in nature^{31,32}.
- ²³ V. N. Staroverov, G. E. Scuseria, J. Tao, and J. P. Perdew, *The Journal of Chemical Physics* **119**, 12129 (2003).
- ²⁴ L. A. Curtiss, K. Raghavachari, P. C. Redfern, and J. A. Pople, *The Journal of Chemical Physics* **112**, 7374 (2000).
- ²⁵ Y. Zhao, J. Pu, B. J. Lynch, and D. G. Truhlar, *Physical Chemistry Chemical Physics*. **6**, 673 (2004).
- ²⁶ B. J. Lynch, , and D. G. Truhlar, *The Journal of Physical Chemistry A* **107**, 8996 (2003).
- ²⁷ W. Koch and M. C. Holthausen, *A chemist's guide to density functional theory* (John Wiley & Sons, 2015).
- ²⁸ C. S. López, O. N. Faza, S. L. Estévez, and A. R. de Lera, *Journal of Computational Chemistry* **27**, 116 (2006).
- ²⁹ L. Ruddigkeit, R. van Deursen, L. C. Blum, and J.-L. Reymond, *Journal of Chemical Information and Modeling* **52**, 2864 (2012).
- ³⁰ T. Fink, H. Bruggesser, and J.-L. Reymond, *Angewandte Chemie International Edition* **44**, 1504 (2005).
- ³¹ T. Bereau and O. A. von Lilienfeld, *The Journal of Chemical Physics* **141**, 034101 (2014).
- ³² R. A. DiStasio, O. A. von Lilienfeld, and A. Tkatchenko, *Proceedings of the National Academy of Sciences* **109**, 14791 (2012).